Real-Time Implementation and Evaluation of Computed-Torque Scheme

Pradeep K. Khosla and Takeo Kanade

CMU-RI-TR-87-6

Department of Electrical and Computer Engineering
The Robotics Institute
Carnegie Mellon University
Pittsburgh, Pennsylvania 15213

March 1987

This research is based upon the work supported by the National Science Foundation under Grant ECS-8320364.

Table of Contents

Abstract

This paper presents the experimental results of the real-time performance of model-based control algorithms. We compare the computed-torque scheme which utilizes the complete dynamics model of the manipulator with the independent joint control scheme which assumes a decoupled and linear model of the manipulator dynamics. The two manipulator control schemes have been implemented on the CMU DD Arm II with a sampling period of 2 ms. We discuss the design of controller gains for both the computed-torque and the independent joint control schemes and establish a framework for comparing their trajectory tracking performance Our investigation shows that the computed-torque scheme outperforms the independent joint control scheme as long as there is no torque saturation in the actuators. Based on our experimental results, we conclusively establish the importance of compensating for the nonlinear Coriolis and centrifugal forces even at low speeds of operation. This represents an important result because it serves to resolve the controversy about the need to compensate for these forces at low speeds of operation.

1. Introduction

In this paper we present the experimental results of the real-time performance of manipulator control algorithms using the full dynamics model. We compare the computed-torque scheme which utilizes the complete dynamics model of the manipulator with the independent joint control scheme. The control schemes have been implemented on the CMU DD Arm II with a sampling period of 2 ms.

Although many simulation results have been presented, the real-time implementation and performance of model-based control schemes with high control sampling rates had not been demonstrated on actual manipulators, until recently [8, 9, 1]. The main reasons for this are:

1. Even though the recent Newton-Euler recursive formulation of the dynamics reduced the amount of computation, its real-time use with a high sampling rate has not yet been practical for the commercially available microprocessors.

2. It is difficult to obtain the dynamic parameters of the robot, such as the link inertias and the center-of-gravity vectors, because research in this area has been lacking.

3. In addition to inertial, centrifugal/Coriolis, and gravitational forces that must be correctly modeled, arm dynamics involve other components of forces, such as static and dynamic friction, which vary due to conditions and thus are hard to predict or model. Since such unpredictable components tend to be large in the nondirect-drive arms, they hamper the efficacy of the computed-torque method.

One of the goals of the CMU Direct-Drive Arm II [13] project is to overcome the above mentioned difficulties and demonstrate the effect of full dynamics compensation on the real-time trajectory tracking of manipulators. For the real-time computation of the inverse dynamics, we have developed a high-speed and powerful computational environment. The computation of inverse dynamics has been customized for the CMU DD Arm II and a computation time of 1 ms has been achieved [5]. To obtain an accurate model we have computed and measured the various parameters from the engineering drawings of the CMU DD Arm II by modeling each link as a composite of hollow and solid cylinders, prisms, and rectangular parallelopipeds. We have also proposed an algorithm to identify the dynamics parameters [7] which has been implemented on the CMU DD Arm II. The results of the experimental implementation of our identification algorithm are presented in [6]. Finally, the negligible friction in our direct-drive arm especially makes it suitable to test the efficacy of the computed-torque scheme.

This paper is organized as follows: In Section 2, we present an overview of the manipulator control schemes that have been implemented and evaluated on the CMU DD Arm II. The experiments to determine the characteristics of the individual joint drive systems are described in Section 3 and the design of controllers is discussed in Section 4.

The real-time experimental results are presented and interpreted in Section 5 and conclusions are drawn in Section 6. In the Appendix, we describe our experimental hardware set-up.

2. Manipulator Control Techniques

The robot control problem revolves around the computation of the actuating joint torques/forces to follow the desired trajectory. The dynamics of a manipulator are described by a set of highly nonlinear and coupled differential equations. The complete dynamic model of an N degrees-of-freedom manipulator is described by:

$$\tau = \mathbf{D}(\theta)\ddot{\theta} + \mathbf{h}(\theta,\dot{\theta}) + \mathbf{g}(\theta) \tag{1}$$

where τ is the N-vector of the actuating torques; $\mathbf{D}(\theta)$ is the $N \times N$ position dependent manipulator inertia matrix; $\mathbf{h}(\theta,\dot{\theta})$ is the N-vector of Coriolis and centrifugal torques; $\mathbf{g}(\theta)$ is the N-vector of gravitational torques; and $\ddot{\theta}$, $\dot{\theta}$ and θ are N-vectors of the joint accelerations, velocities and positions, respectively.

This complex description of the system makes the design of controllers a difficult task. To circumvent the difficulties the control engineer often assumes a simplified model to proceed with the controller design. Industrial manipulators are usually controlled by conventional PID-type independent joint control structures designed under the assumption that the dynamics of the links are uncoupled and linear. The controllers based on such an overly simplified dynamics model result in low speeds of operation and overshoot of the end-effector.

To improve the performance of the PID controllers, researchers have investigated model-based control schemes which attempt to compensate for the nonlinearities and the mismatch in the dynamical description of the robot. One of the model-based techniques is the *feedforward dynamics compensation* method which computes the desired torques from the given trajectory and injects these torques as feedforward control signals. Independent joint feedback controllers are then added with the intention of compensating for the small coupling torques arising out of the mismatch in the dynamics of the model and the real arm [3, 11]. More thorough compensation can be achieved by the *computed-torque* technique in which the dynamics compensation is included in the feedback loop to decouple and linearize the manipulator dynamics. This technique has been extended to operate in the Cartesian space and is called *resolved-acceleration* scheme [10].

We have implemented computed-torque and the independent joint control schemes and compared their real-time performance. To establish a framework for comparing the performance these two schemes, we consider the control law in two steps; computation of

the commanded acceleration and computation of the control torque. The commanded joint accelerations $\mathbf{u}_i$ can be computed in one of the following three ways:

$$\mathbf{u}_1 = \mathbf{K}_p(\theta_d - \theta) - \mathbf{K}_v\dot{\theta} \tag{2}$$

$$\mathbf{u}_2 = \mathbf{K}_p(\theta_d - \theta) + \mathbf{K}_v(\dot{\theta}_d - \dot{\theta}) \tag{3}$$

$$\mathbf{u}_3 = \mathbf{K}_p(\theta_d - \theta) + \mathbf{K}_v(\dot{\theta}_d - \dot{\theta}) + \ddot{\theta}_d \tag{4}$$

where $\mathbf{K}_p$ and $\mathbf{K}_v$ are $N \times N$ diagonal position and velocity gain matrices, respectively. The N-vectors θ_d and θ are the desired and measured joint positions, respectively, and the " $\cdot$ " indicates the time derivative of the variables. Whereas only the position error and the velocity damping is used in equation (2), the commanded acceleration signal in equation (3) uses a velocity feedforward term, and the commanded acceleration signal in equation (4) uses both the velocity and acceleration feedforward terms. The idea is to increase the speed of response by incorporating a feedforward term.

The fundamental difference between the independent joint control schemes and the model-based schemes lies in the second step in the control law, i.e., the method of computing the applied control torque signals from the commanded acceleration signals. If the vector of actuating joint torques τ is computed from the commanded acceleration signal under the assumption that the joint inertias are constant, then we obtain an independent joint control scheme. On the other hand, if the actuating torques τ are computed from the *inverse dynamics* model in equation (1) then we obtain the computed-torque scheme.

Specifically, we have implemented and evaluated the real-time performance of the following three control schemes:

Independent Joint Control (IJC) In this scheme, linear PD control laws were designed for each joint based on the assumption that the joints are decoupled and linear. The control torque τ applied to the joints at each sampling instant is:

$$\tau = \mathbf{J}\mathbf{u}_i \tag{5}$$

where $\mathbf{J}$ is the constant $N \times N$ diagonal matrix of link inertias at a typical position.

Computed-Torque Control (CT) This scheme utilizes nonlinear feedback to decouple the manipulator. The control torque τ is computed by the inverse dynamics equation in equation (1), using the commanded acceleration $\mathbf{u}_i$ instead of the measured acceleration $\ddot{\theta}$:

$$\tau = \tilde{\mathbf{D}}(\theta)\mathbf{u}_i + \tilde{\mathbf{h}}(\theta,\dot{\theta}) + \tilde{\mathbf{g}}(\theta) \tag{6}$$

where the " $\sim$ " indicates that the estimated values of the dynamics parameters are used in the computation.

Computed-Torque Control with Reduced Dynamics (RCT) The effect of the velocity dependent Coriolis and centrifugal term $\mathbf{h}(\theta,\dot{\theta})$ on the trajectory tracking performance of manipulators has been a subject of controversy [4, 12]. To study this effect, we compute the control torque excluding the velocity dependent terms in the inverse dynamics in equation (6). The control torque is therefore:

$$\tau = \tilde{\mathbf{D}}(\theta)\mathbf{u}_i + \tilde{\mathbf{g}}(\theta) \tag{7}$$

For the sake of brevity we will henceforth use the abbreviations IJCi, CTi and RCTi to refer to the independent joint control, the computed-torque, and the reduced computed-torque schemes, respectively. The number i in the abbreviations denotes the method of computing the commanded accelerations from either (2), (3) or (4). For example, CT3 would imply that the control torque is computed as:

$$\tau = \tilde{\mathbf{D}}(\theta)\mathbf{u}_3 + \tilde{\mathbf{h}}(\theta,\dot{\theta}) + \tilde{\mathbf{g}}(\theta)$$

The real-time control experiments using these schemes have been performed with the CMU DD Arm II. Before proceeding with the design of the controller gain matrices, we need to determine the order and transfer function of the individual joint drive systems.

3. Characteristics of the Joint Drive Systems of CMU DD Arm II

The application of the control law in equation (6) is based on the assumption that each individual link can be modeled as a double integrator and that the joint drive is a torque controlled device. The CMU DD Arm II has very little friction, and is driven by brushless DC-torque motors with the amplifiers which control motor current rather than voltage or speed. To ensure that the above assumption is satisfied, we have identified the characteristics of the joint drive systems.

We conducted the open-loop small-signal frequency response analysis and identified the continuous-time transfer function of each joint. Since our sampling period of 2 ms is about 10 times smaller than the dominant mechanical time constant of the system we assume that the effects of sampling are not evident in the input-output response of the system: this assumption is indeed supported by the experimental results.

The transfer function obtained from the frequency response analysis is valid only for small displacements around a particular position of each joint. For convenience, we chose this as the home position of the CMU DD Arm II where all the joint displacements are zero [5]. We allowed only one joint to move under a sinusoidal excitation signal while all the other joints were mechanically locked. The sinusoidal excitation was generated on the microprocessor and applied through the digital-to-analog converters at a control sampling period of 2 ms. Sinusoidal signals ranging in frequency from 0.1 Hz to 10 Hz were applied and the input signal and the output position recorded. From the input-output measurements we generated the Bode plots wherein the log-magnitude plot had a slope of -40 db/decade and the phase angle was approximately -180 degrees, which suggested that the single link system is indeed a double integrator. The identified transfer functions are depicted in Table . This test also supports our assumptions that:

1. Our control sampling period is much smaller than the dominant time constant of a system, and the resulting input-output behavior can be characterized in the Laplace s-plane.

2. The effects of the armature inductance of the motor and the time constant of the amplifier are negligible and the joint drive is a torque controlled device.

3. The effect of viscous (or friction) damping is negligible.

Item 1 is an important result because it permits us to proceed with the controller design in the s-domain and allows us to specify the controller criteria in terms of the desired damping.

To verify that the modeled amplifier gain and the torque constant of the motor are accurate, we computed the manipulator inertia matrix $\mathbf{D}(\theta)$ at the home position of the CMU DD Arm II. The computed diagonal elements of this matrix were within 10% of the identified joint inertias (in Table) and support our assumption about the amplifier gains and the motor torque constants.

4. Controller Design

The performance of the nonlinear CT scheme and the linear IJC scheme can be compared only if the same criteria are used for design of the controller gain matrices. Fortunately, this is possible because the gain matrices $\mathbf{K}_p$ and $\mathbf{K}_v$ appear only in the commanded accelerations which are the same (Equations (2)-(4)) for both CT and IJC

schemes. Thus, whether we implement the simplistic independent joint control scheme or the sophisticated computed-torque scheme, we are faced with the problem of designing the gain matrices $\mathbf{K}_p$ and $\mathbf{K}_v$. These matrices are chosen to satisfy the specified output response criterion.

4.1. Design of Gain Matrices for Independent Joint Control

The closed loop transfer function relating the input θ_{jd} to the measured output θ_j for joint j is:

$$\frac{\theta_j}{\theta_{jd}} = \frac{s^2\delta + s\gamma k_{vj} + k_{pj}}{s^2 + k_{vj}s + k_{pj}} \tag{8}$$

where γ=1 if velocity feedforward is included and zero otherwise, and δ=1 if acceleration feedforward is included and zero otherwise. The closed-loop characteristic equation in all the three cases is,

$$s^2 + k_{vj}s + k_{pj} = 0 \tag{9}$$

and its roots are specified to obtain a stable response. The complete closed-loop response of the system is governed by both the zeros and the poles of the system. In the absence of any feedforward terms, the response is governed by the poles of the transfer function.

Since it is desired that none of the joints overshoot the commanded position or the response be critically damped, our choice of the matrices $\mathbf{K}_p$ and $\mathbf{K}_v$ must be such that their elements satisfy the condition:

$$k_{vj} = 2\sqrt{k_{pj}} \qquad \text{for j} = 1,\ldots..,6 \tag{10}$$

Besides, in order to achieve a high disturbance rejection ratio or high stiffness it is also necessary to choose the position gain matrix $\mathbf{K}_p$ as large as possible which results in a large $\mathbf{K}_v$.

In practice, however, the choice of the velocity gain $\mathbf{K}_v$ is limited by the noise present in the velocity measurement. We determined the upper limit of the velocity gain experimentally: we set the position gain to zero and increased the velocity gain of each joint until the unmodeled high-frequency dynamics of the system were excited by the noise introduced in the velocity measurement. This value of $\mathbf{K}_v$ represents the maximum allowable velocity gain. We chose 80% of the maximum velocity gain in order to obtain as high value of the position gain as possible and still be well within the stability limits with respect to the unmodeled high frequency dynamics. The elements of the position gain matrix $\mathbf{K}_p$ were computed to satisfy the critical damping condition in equation (10) and also achieved the maximum disturbance rejection ratio. The elements of the velocity and

position gain matrices used in the implementation of the control schemes are listed in Table .

We also performed a small-signal step response test of the individual joints to check the performance of the linear controllers for the joints. Each joint was commanded with a step input of amplitude 0.1 rad while the other joints were locked and the input-output response plotted. We used the gain values listed in Table and confirmed that the response of the system was indeed critically damped.

4.2. Design of Gain Matrices for Computed-Torque Scheme

The basic idea behind the computed-torque scheme is to achieve dynamic decoupling of all the joints using nonlinear feedback. If the dynamic model of the manipulator is described by equation(1) and the applied control torque is computed according to equation (6), then the following closed-loop system is obtained:

$$\ddot{\theta} = \mathbf{u}_i - [\tilde{\mathbf{D}}]^{-1}\{[\mathbf{D} - \tilde{\mathbf{D}}]\ddot{\theta} + [\mathbf{h} - \tilde{\mathbf{h}}] + [\mathbf{g} - \tilde{\mathbf{g}}]\}$$

where the functional dependencies on θ and $\dot{\theta}$ have been omitted for the sake of clarity. If the dynamics are modeled exactly, that is, $\tilde{\mathbf{D}}$=$\mathbf{D}$, $\tilde{\mathbf{h}}$=$\mathbf{h}$ and $\tilde{\mathbf{g}}$=$\mathbf{g}$, then the decoupled closed loop system is described by

$$\ddot{\theta} = \mathbf{u}_i.$$

Upon substituting the right hand side of either equation (2), (3) or (4) in the above equation, we obtain the closed-loop input-output transfer function of the system. The closed-loop characteristic equation in all the three cases is:

$$s^2 + k_{vj}s + k_{pj} = 0 \tag{11}$$

where k_{vj} and k_{pj} are the velocity and position gains for the *j-th* joint. Upon comparing equation (9) and (11), we obtain the relationships

$k_{pj}[CT]$=$k_{pj}[IJC]$ and $k_{vj}[CT]$=$k_{vj}[IJC]$

which suggest that the gains of the IJC scheme are also the gains of the CT scheme. This equality must be expected because the closed-loop characteristic equation for both the independent joint control and the computed-torque scheme is the same.

5. Experiments and Results

5.1. Trajectory Selection and Evaluation Criteria

Since the DD Arm II is a highly nonlinear and coupled system it is impossible to characterize its behavior from a particular class of inputs, unlike linear systems for which a specific input (such as a unit step or a ramp) can be used to design and evaluate the

controllers. Thus an important constituent of the experimental evaluation of robot control schemes is the choice of a class of inputs for the robot. The criteria for selecting the joint trajectories is detailed in [6].

For evaluating the performance of robot control schemes, we use the dynamic tracking accuracy. This is defined as the maximum position and velocity tracking error along a specified trajectory.

5.2. Real-Time Results

We have implemented the nine control schemes IJCi, CTi and RCTi (for $i = 1, 2$ and 3), presented in Section 2, and evaluated their real-time performance on the six degrees-of-freedom CMU DD Arm II. Because of lack of space, we present our results for two simple but illustrative trajectories.

The first trajectory is chosen to be simple and relatively slow but capable of providing insight into the effect of dynamics compensation. In this trajectory only joint 2 moves while all the other joints are commanded to hold their zero positions and can be envisioned from the schematic diagram in Figure . Joint 2 is commanded to start from its zero position and to reach the position of 1.5 rad in 0.75 seconds; it remains at this position for an interval of 0.75 seconds after which it is required to return to its home position in 0.75 seconds. The points of discontinuity, in the trajectory, were joined by a fifth-order polynomial to maintain the continuity of position, velocity and acceleration along the three segments. The desired position, velocity and acceleration trajectories for joint 2 are depicted in Figure 1. The maximum velocity and acceleration to be attained by joint 2 are 2 rad/sec and 6 rad/sec^2, respectively.

The position and velocity tracking curves for the schemes CT3, IJC3 and RCT3 are depicted in Figures 3 through 8. The corresponding position and velocity tracking errors in the three schemes for each joint are shown in Figures 9 through 14. To give an idea of the relative performances, the maximum position and velocity tracking errors of each joint are depicted in Table . We note that CT3 had the least position tracking error while IJC3 displayed the maximum error for all the three joints shown. The same can be said in the velocity tracking wherein CT3 exhibits the least tracking error while IJC3 has the maximum tracking error amongst all the three schemes. Similar results were also obtained for the last three wrist joints but have not been included for the sake of brevity.

Writing the dynamic equations for the first three degrees-of-freedom of the CMU DD Arm II provides an insight to interpret the results:

$$\tau_1 = d_{11}\ddot{\theta}_1 + d_{12}\ddot{\theta}_2 + d_{13}\ddot{\theta}_3 + h_{133}\dot{\theta}^2{}_3 + h_{122}\dot{\theta}^2{}_2 \quad (12)$$
$$+ 2h_{123}\dot{\theta}_2\dot{\theta}_3 + 2h_{113}\dot{\theta}_1\dot{\theta}_3 + 2h_{112}\dot{\theta}_1\dot{\theta}_2$$

$$\tau_2 = d_{21}\ddot{\theta}_1 + d_{22}\ddot{\theta}_2 + d_{23}\ddot{\theta}_3 + h_{233}\dot{\theta}^2{}_3 + h_{223}\dot{\theta}_2\dot{\theta}_3 \quad (13)$$
$$+ 2h_{213}\dot{\theta}_1\dot{\theta}_3 - h_{211}\dot{\theta}^2{}_1$$

$$\tau_3 = d_{31}\ddot{\theta}_1 + d_{32}\ddot{\theta}_2 + d_{33}\ddot{\theta}_3 - h_{322}\dot{\theta}^2{}_2 \quad (14)$$
$$- 2h_{312}\dot{\theta}_1\dot{\theta}_2 - h_{311}\dot{\theta}^2{}_1 + g_3$$

The coefficients d_{ij}, h_{ijk} and g_i are functions of the joint position vector θ and are detailed in [7].

The applied torque signals for the three schemes are shown in Figures 15–17. Further, decomposition of the applied torques in CT3 into the inertial, the centrifugal and Coriolis, and the gravity components of joints 1 through 3 is presented in Figures 18–20. First of all, we note that the applied torque for joint 1 has a profile similar to the desired acceleration of joint 2 except during the periods of constant speed (0.75 to 1.0 sec and 2.25 to 2.5 sec) in the trajectory. This suggests that the inertial coupling torque $d_{12}\ddot{\theta}_2$ dominates along most part of the trajectory. This is further supported by the profile of the inertial torque component in Figure 18; the small deviations are due to the velocity and position tracking errors which contribute to the computed joint acceleration in equation (4). During the periods of constant speed the applied torque curve is not similar to the desired acceleration profile because the centrifugal and the Coriolis components dominate. The exclusion of these velocity dependent torque components in RCT3 therefore results in increased velocity tracking errors as observed in Figure 10. This demonstrates the importance of including the velocity dependent terms in the dynamics for trajectory tracking even at low joint velocities.

Next, the applied torque for joint 3 is also dominated by the velocity dependent $h_{223}\dot{\theta}^2{}_2$ term in (14) and the inertial torque component arises from the error in position and velocity tracking in the first three joints as evidenced in Figure 20.

Finally, in the case of joint 2 the applied torque curve is similar to the profile of its desired acceleration. This suggests that the applied torque basically consists of the inertial torque component. In equation (13) there is no term in $\dot{\theta}^2{}_2$ and hence hardly any velocity dependent torque component. In fact, we observe that the centrifugal and Coriolis torque component is zero in the decomposition of joint 2 torque as shown in Figure 19. The

increase in the position tracking error, in Figure 11, and the deterioration of velocity tracking, in Figure 12 is basically due to the tracking errors in joints 1 and 3 which are reflected as inertial coupling terms in the applied torque of joint 2.

We have also conducted experiments with more complex trajectories which involve motions of all joints. Figure 21 is such an example, wherein the motions of joint 2 are depicted for CT3 and IJC3, and demonstrates the superior tracking performance of the computed-torque method to individual joint control method. We have also been able to analyze the effect of various torque components in trajectory tracking.

In our experiments, we have noticed an improvement in the trajectory tracking performance of the independent joint control scheme when the reference acceleration is also included as a feedforward signal together with the reference velocity as in equation (4). We have thus compared the best performance of the independent joint control scheme with the computed-torque scheme.

6. Conclusions

In this paper, we have presented the first implementation of the computed-torque scheme and compared its real-time performance with the conventional independent joint control scheme. We have discussed the design of the controller gains for both the independent joint control and the computed-torque schemes and established a framework for the comparison of their trajectory tracking performance. Our initial investigation shows that the computed-torque scheme clearly outperforms the conventional independent joint control scheme in which no acceleration feedforward is introduced. We have also shown that inclusion of the reference acceleration as a feedforward control signal reduces the tracking lag and the improves the trajectory tracking performance of the independent joint control scheme.

It had been intuitively argued before that the effect of Coriolis and centrifugal forces become important only at high speeds. Our experiments with the trajectory where only joint 2 is moving, however, show that these effects introduce trajectory tracking errors even at small joint velocities. In summary, the computed-torque scheme performs better trajectory tracking than the independent joint control scheme in the absence of torque saturation. In the event of torque saturation, the computed-torque scheme may become unstable if the tracking errors become large. This necessitates generating trajectories by including both the dynamics and the control law.

I. The CMU DD Arm II

We have developed, at CMU, the concept of direct-drive robots in which the links are directly coupled to the motor shaft. This construction eliminates undesirable properties like friction and gear backlash. The CMU DD Arm II [13] is the second version of the

CMU direct-drive manipulator and is designed to be faster, lighter and more accurate than its predecessor CMU DD Arm I [2]. We have used brushless rare-earth magnet DC torque motors driven by current controlled amplifiers to achieve a torque controlled joint drive system. The SCARA-type configuration of the arm reduces the the torque requirements of the first two joints and also simplifies the dynamic model of the arm. To achieve the desired accuracy, we use very high precision (16 bits/rotation) rotary absolute encoders. The arm weighs approximately 70 pounds and is designed to achieve maximum joint accelerations of 10 rad/sec^2.

The hardware of the DD Arm II control system consists of three integral components: the Motorola M68000 microcomputer, the Marinco processor and the TMS-320 microprocessor-based individual joint controllers. We have also developed the customized Newton-Euler equations for the CMU DD Arm II and achieved a computation time of 1 ms by implementing these on the Marinco processor. The details of the customized algorithm, hardware configuration and the numerical values of the dynamics parameters are presented in [5].

Table 1
Transfer Functions and Gains of Individual Links

Joint (j)	Transfer Function ($\frac{1}{J_j s^2}$)	k_{pj}	k_{vj}
1	$\frac{1}{12.3s^2}$	40.0	12.6
2	$\frac{1}{2s^2}$	58.0	15.2
3	$\frac{1}{0.25s^2}$	400.0	40.0
4	$\frac{1}{0.007s^2}$	2800.0	106.0
5	$\frac{1}{0.006s^2}$	1200.0	69.3
6	$\frac{1}{0.0003s^2}$	3000.0	110.0

Table 2
Maximum Tracking Errors for T1

	CT3		RCT3		IJC3	
Joint No.	Pos Error (rads)	Vel Error (rads/sec)	Pos Error (rads)	Vel Error (rads/sec)	Pos Error (rads)	Vel Error (rads/sec)
1	0.022	0.07	0.034	0.13	0.036	0.18
2	0.023	0.16	0.04	0.26	0.032	0.165
3	0.008	0.005	0.015	0.019	0.018	0.09

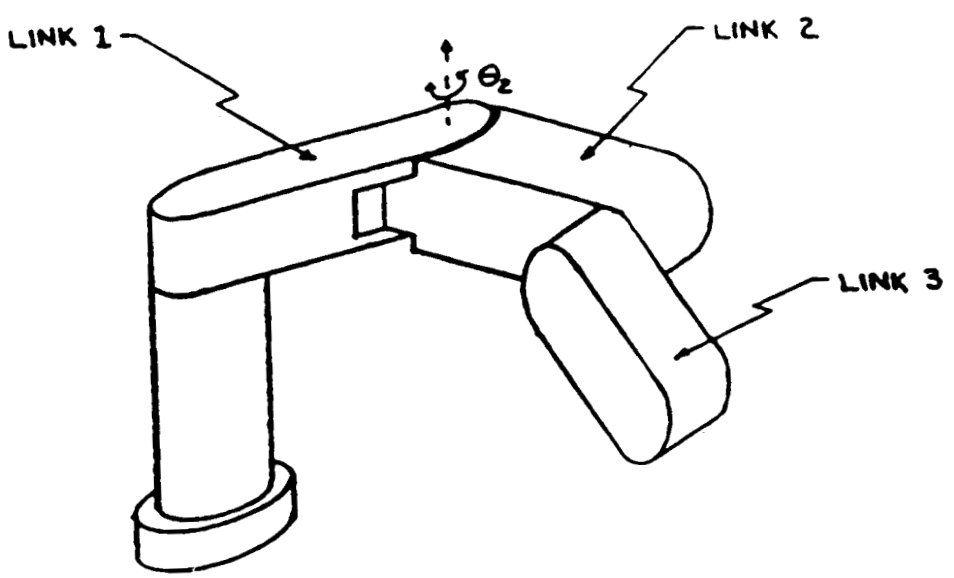

Figure 1: Schematic diagram of 3 DOF DD Arm II

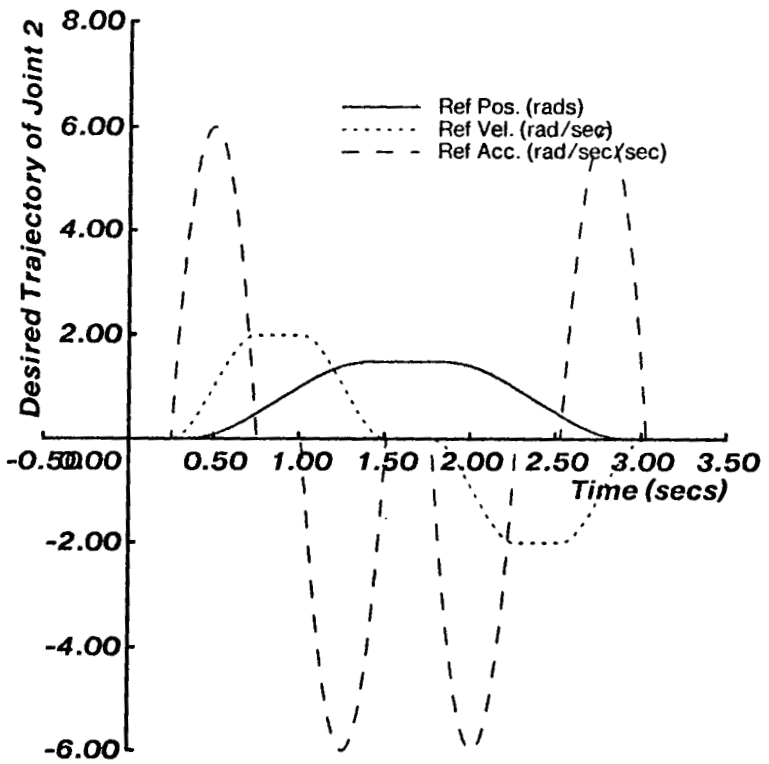

Figure 2: Desired trajectories for joint 2

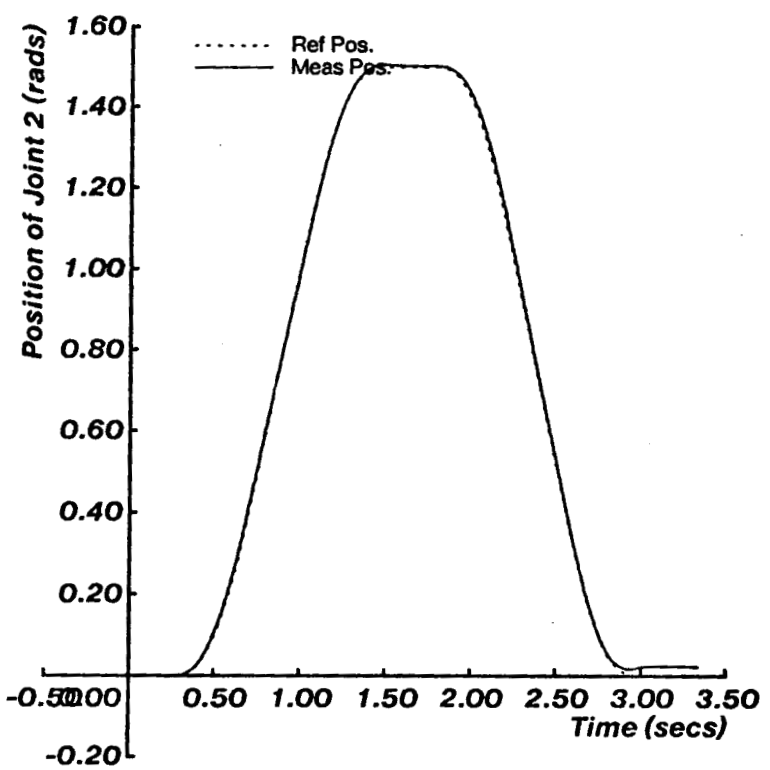

Figure 3: Position tracking in CT3

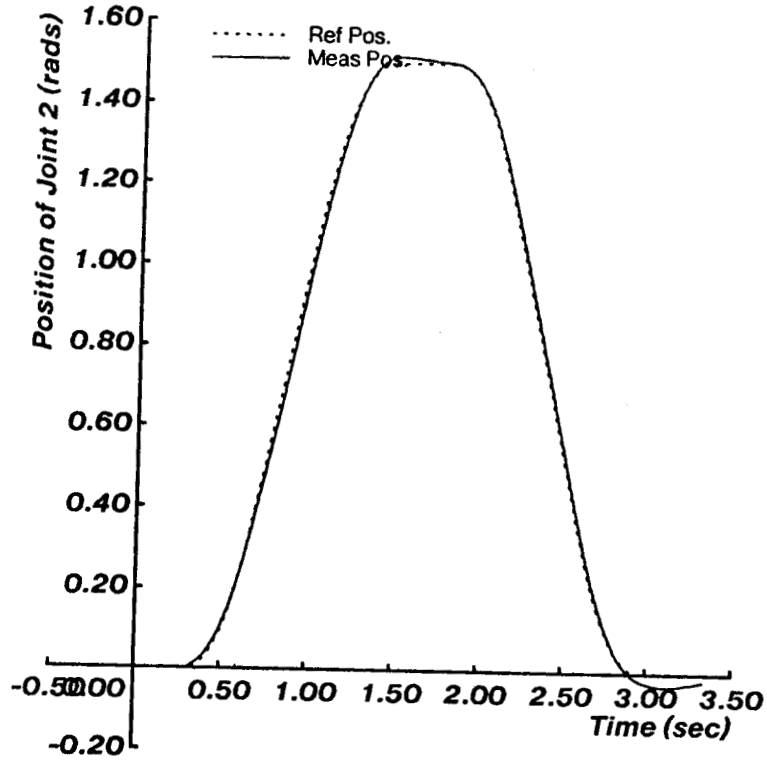

Figure 4: Position tracking in IJC3

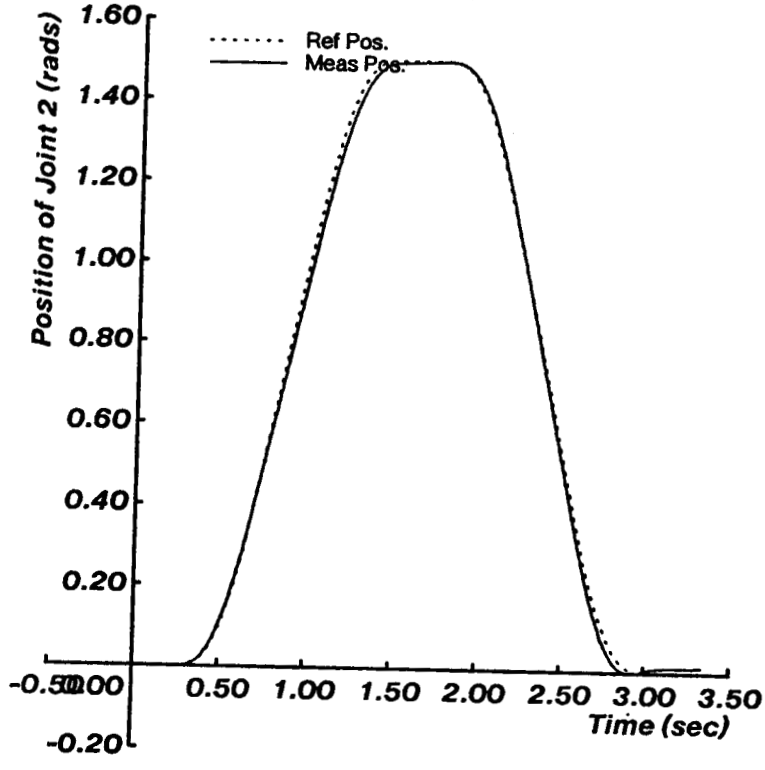

Figure 5: Position tracking in RCT3

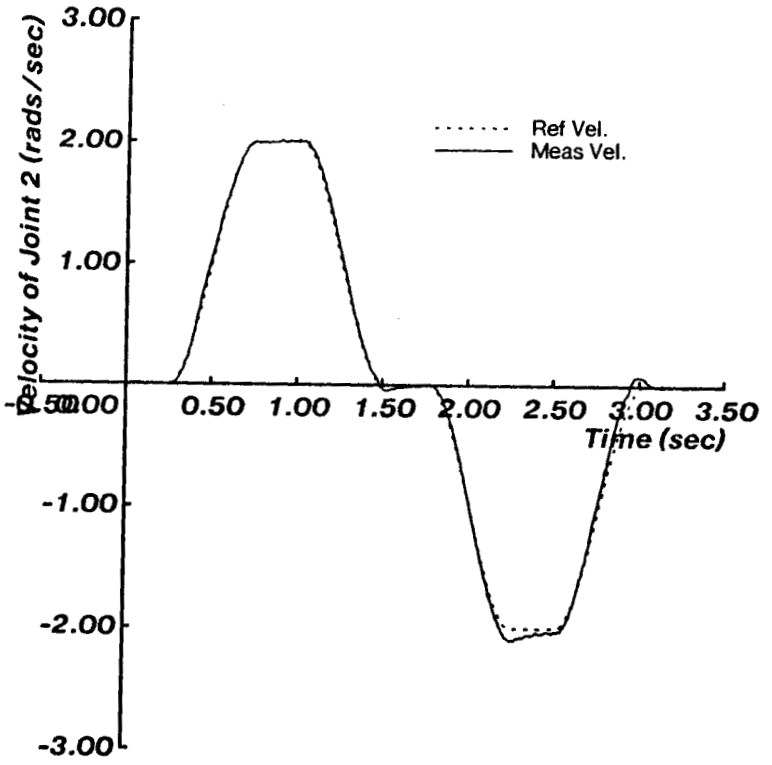

Figure 6: Velocity tracking in CT3

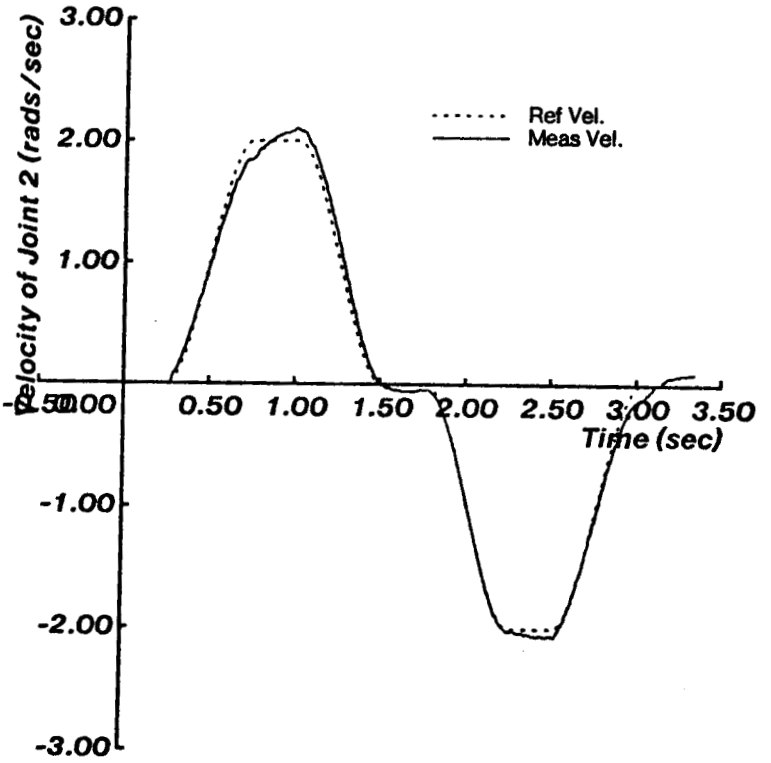

Figure 7: Velocity tracking in IJC3

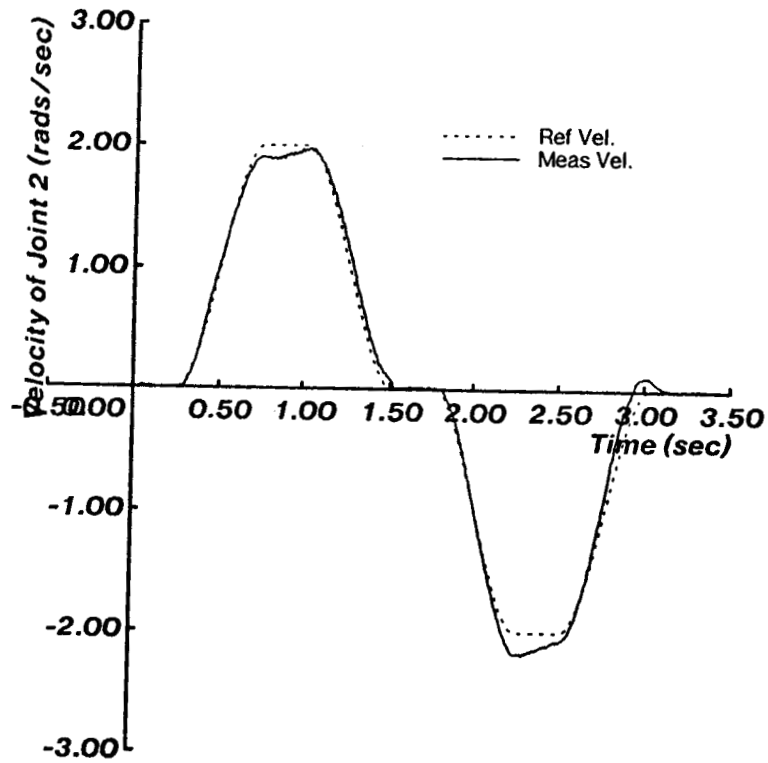

Figure 8: Velocity tracking in RCT3

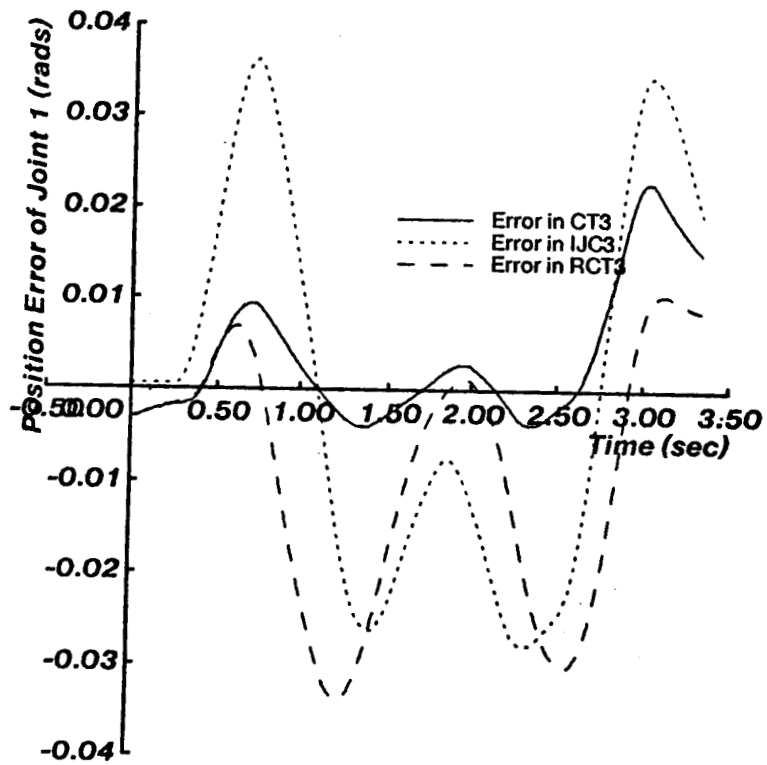

Figure 9: Position tracking errors of joint 1

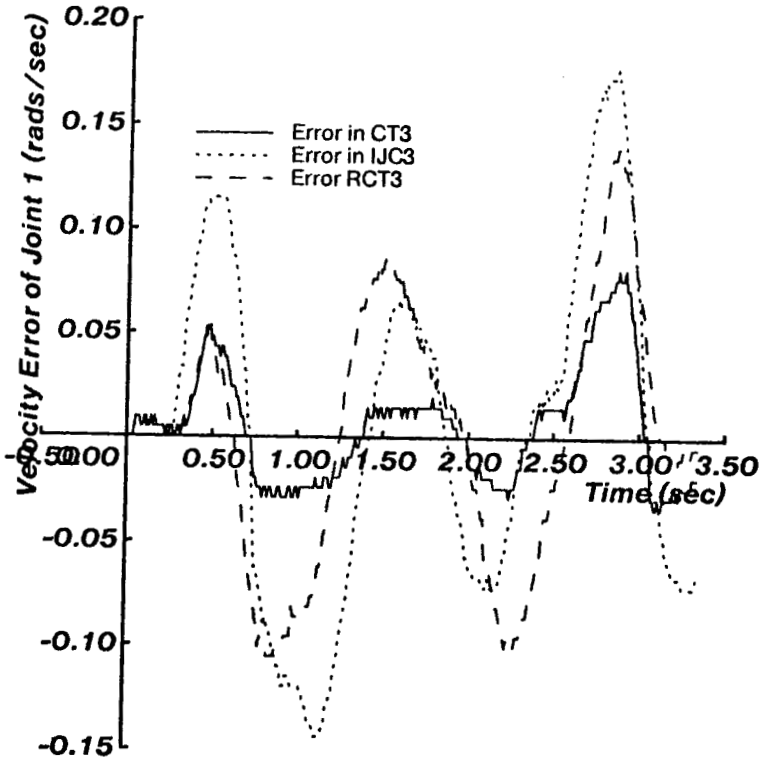

Figure 10: Velocity tracking errors of joint 1

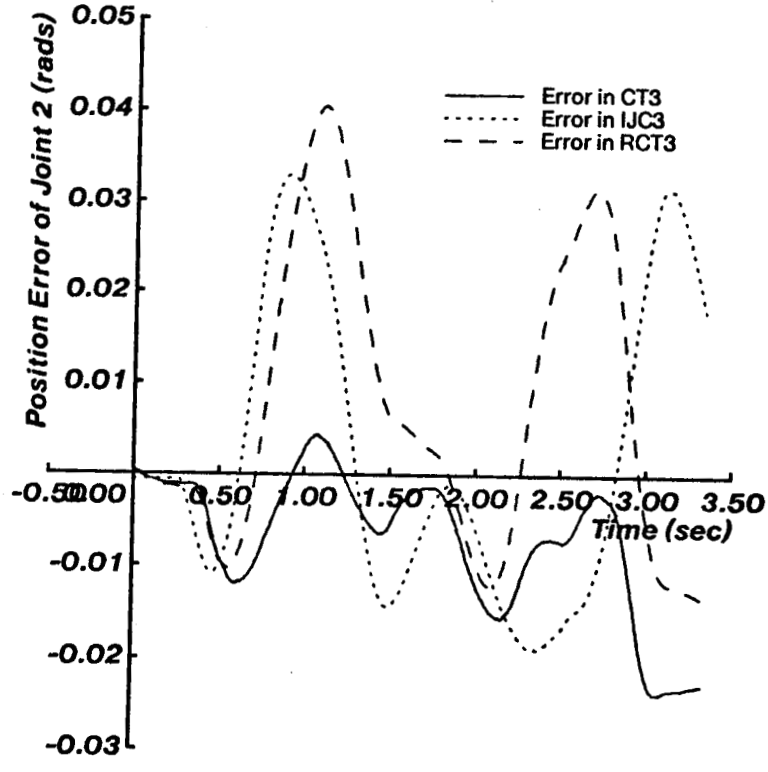

Figure 11: Position tracking errors of joint 2

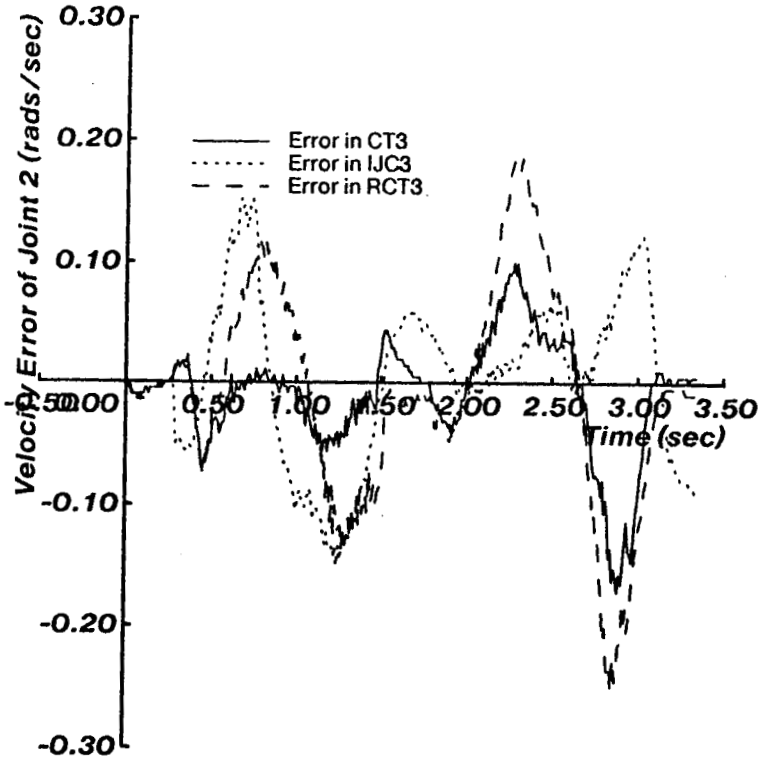

Figure 12: Velocity tracking errors of joint 2

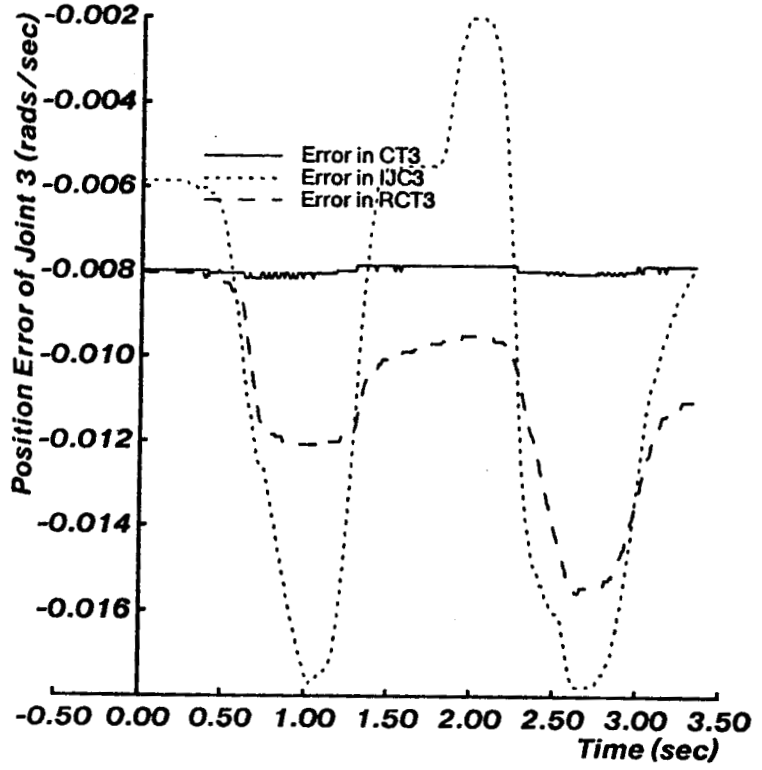

Figure 13: Position tracking errors of joint 3

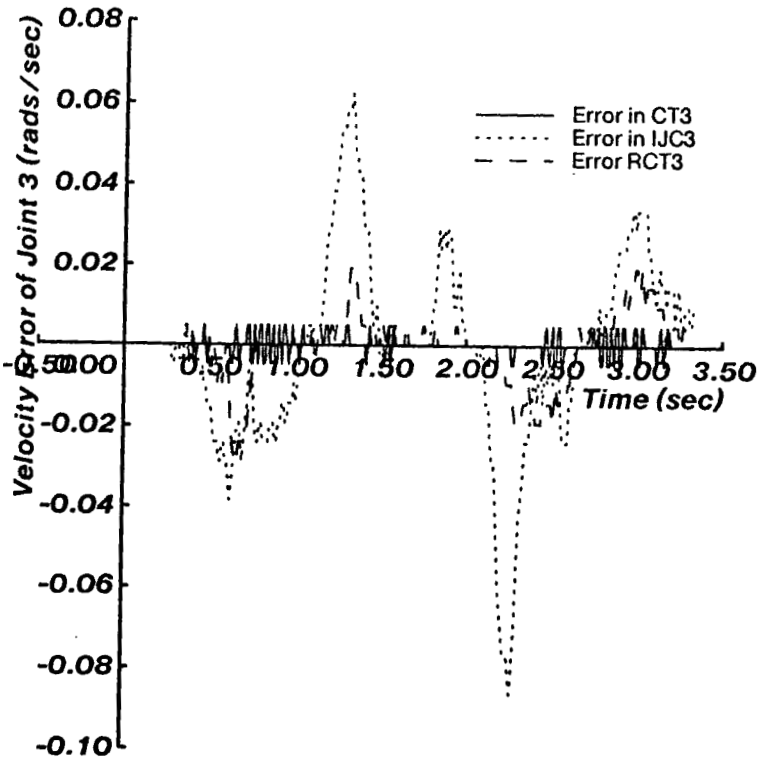

Figure 14: Velocity tracking errors of joint 3

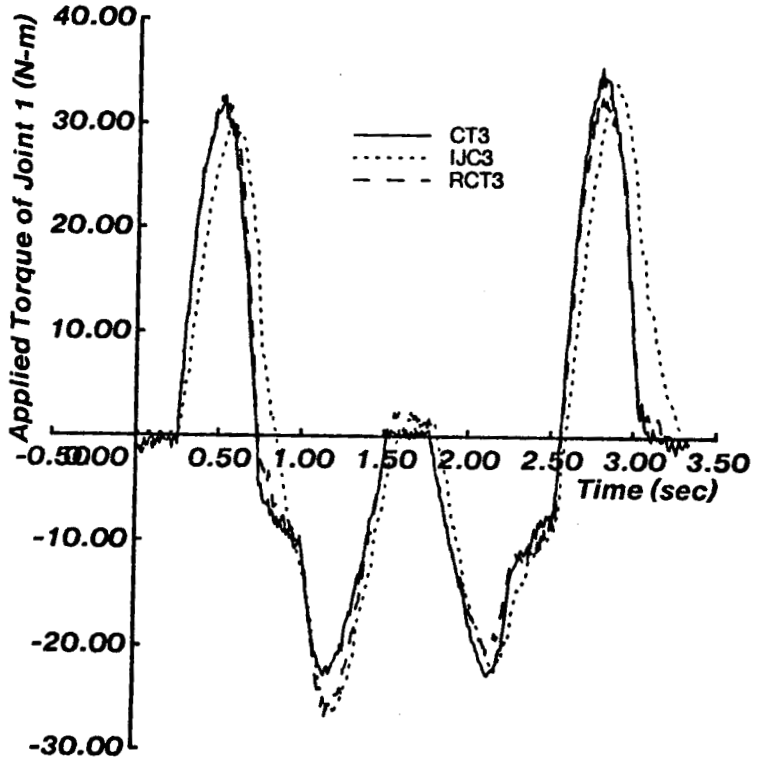

Figure 15: Applied torque of joint 1

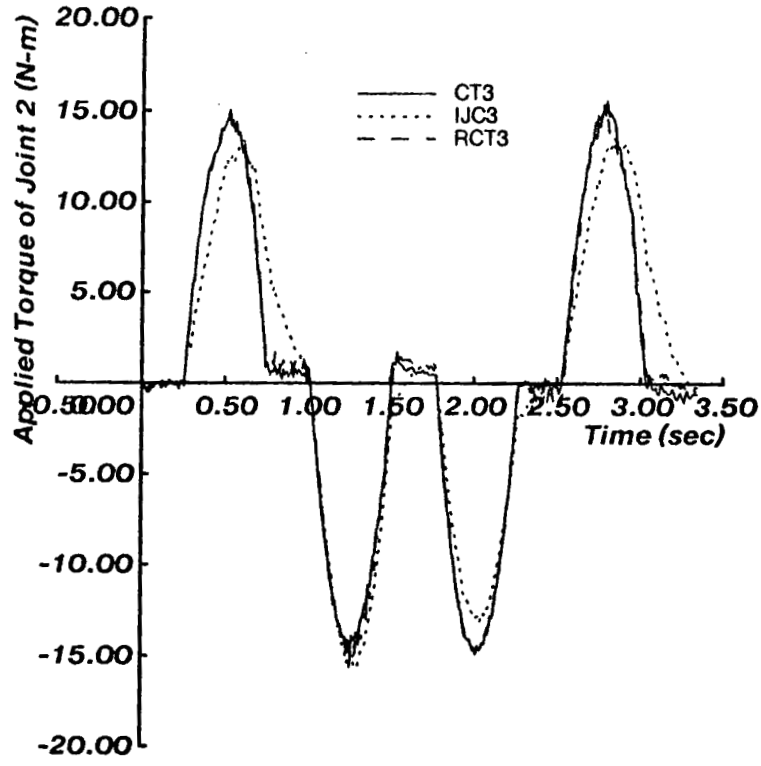

Figure 16: Applied torque of joint 2

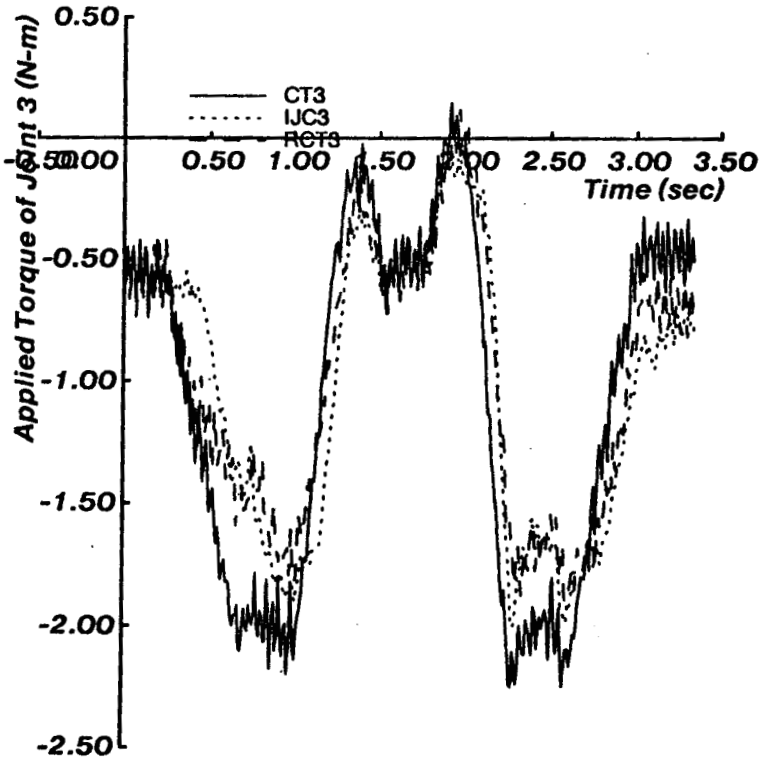

Figure 17: Applied torque of joint 3

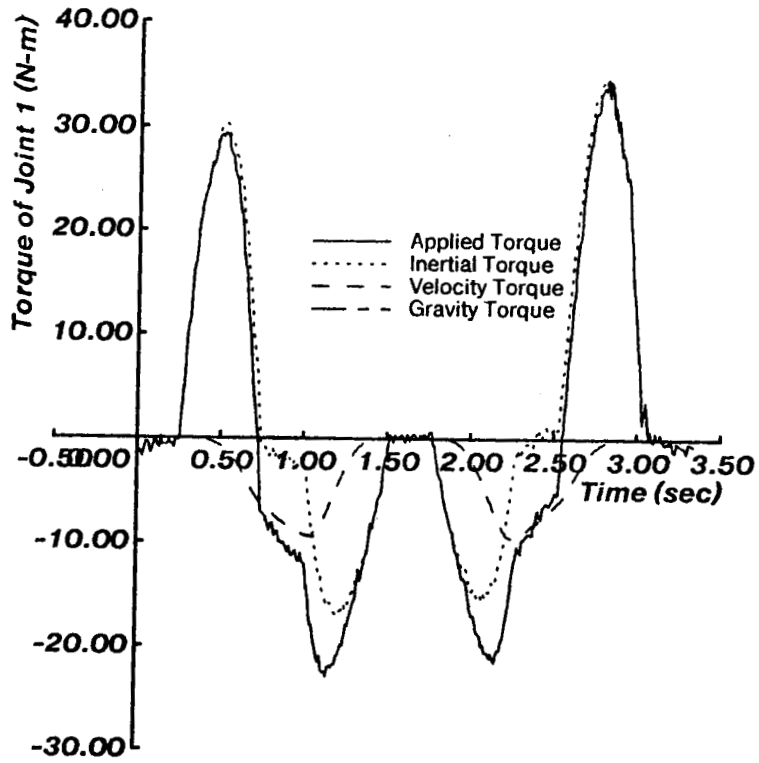

Figure 18: Torque components in CT3

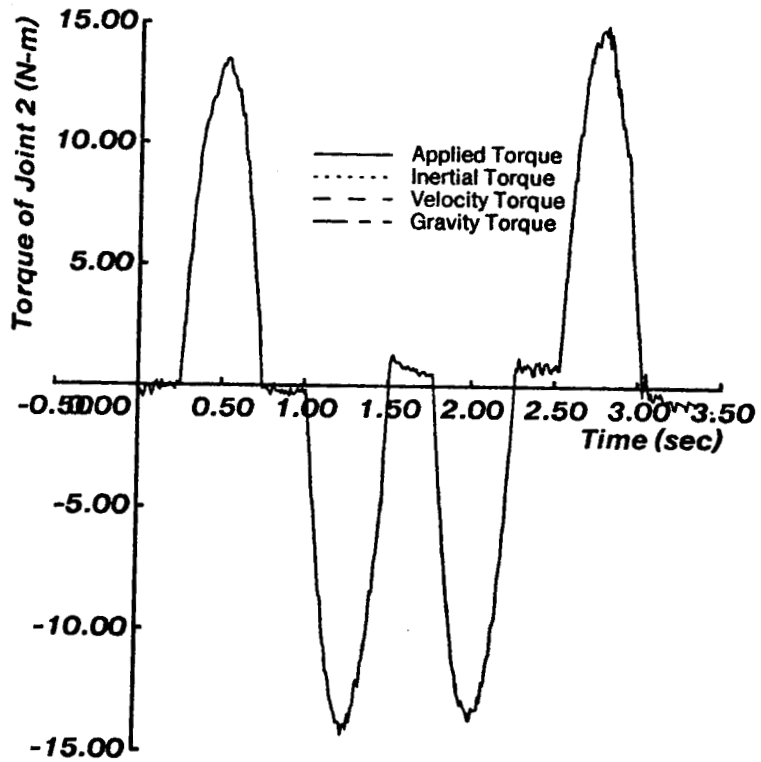

Figure 19: Torque components in CT3

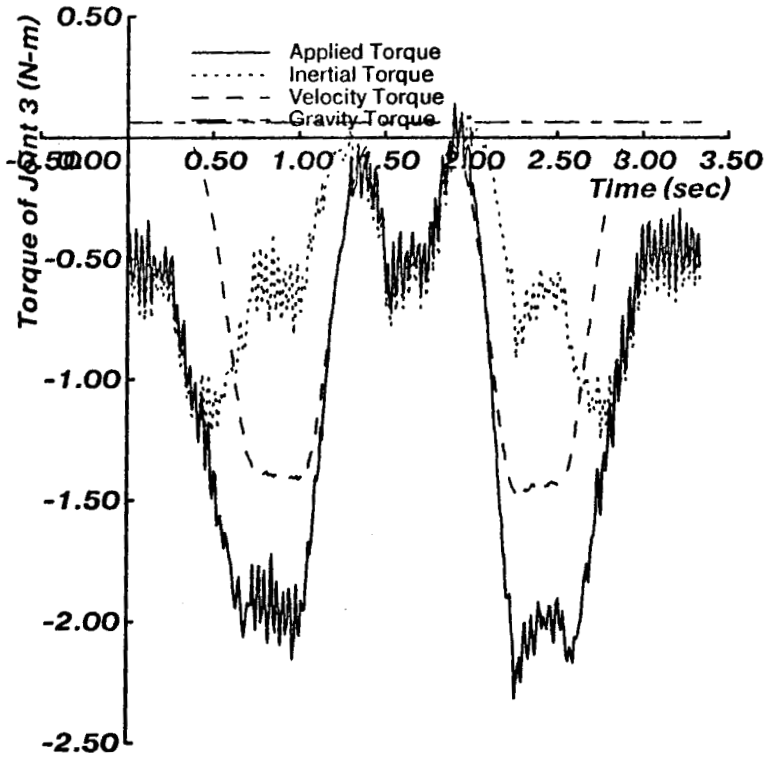

Figure 20: Torque components in CT3

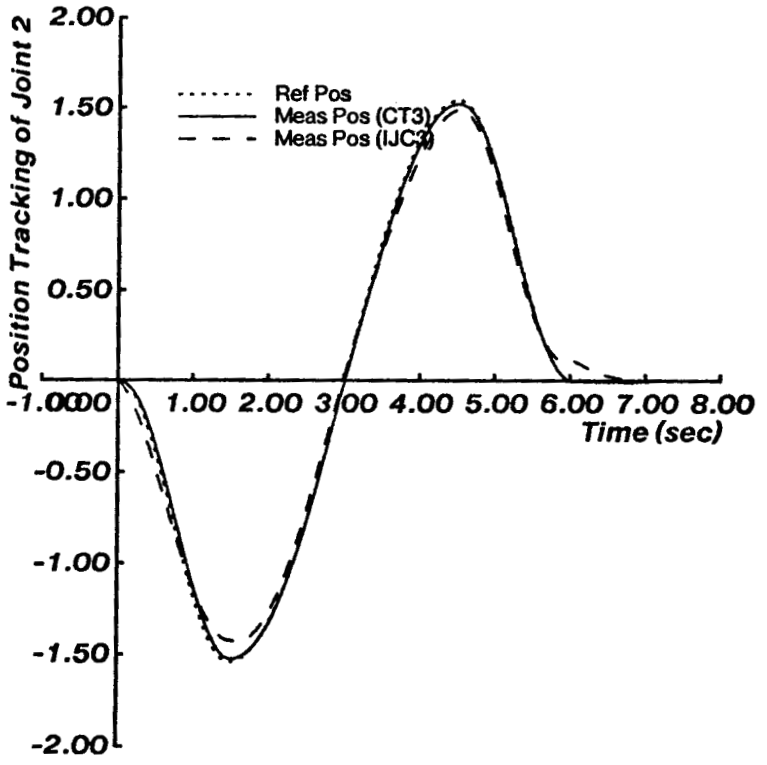

Figure 21: Complex trajectory tracking by CT3, IJC2, and IJC3

References

[1] An, C. H., Atkeson, C. G. and Hollerbach, J. M.
Experimental Determination of the Effect of Feedforward Control on Trajectory Tracking Errors.
In Bejczy, A. K. (editor), *Proceedings of 1986 IEEE Conference on Robotics and Automation*, pages 55-60. IEEE, San Francisco, CA, April 7-10, 1986.

[2] Asada, H. and Kanade, T.
Design of Direct Drive Mechanical Arms.
Journal of Vibration, Stress, and Reliability in Design 105(1):312-316, July, 1983.

[3] Asada, H., Kanade, T. and Takeyama, I.
Control of a Direct-Drive Arm.
Technical Report CMU-RI-TR-82-4, The Robotics Institute, Carnegie-Mellon University, April, 1982.

[4] Hollerbach, J. M.
Dynamic Scaling of Manipulator Trajectories.
Journal of Dynamic Systems, Measurement, and Control 106(1):102-106, March, 1984.

[5] Kanade, T., Khosla, P. K. and Tanaka, N.
Real-Time Control of the CMU Direct Drive Arm II Using Customized Inverse Dynamics.
In Polis, M. P. (editor), *Proceedings of the 23rd IEEE Conference on Decision and Control*, pages 1345-1352. Las Vegas, NV, December 12-14,, 1984.

[6] Khosla, P. K.
Real-Time Control and Identification of Direct-Drive Manipulators.
PhD thesis, Department of Electrical and Computer Engineering, Carnegie-Mellon University, August , 1986.

[7] Khosla, P. K. and Kanade, T.
Parameter Identification of Robot Dynamics.
In Franklin, G. F. (editor), *Proceedings of the 24-th CDC*, pages 1754-1760. Florida, December 11-13, 1985.

[8] Khosla, P. K. and Kanade, T.
Real-Time Implementation and Evaluation of Model-Based Controls on CMU DD ARM II.
In Bejczy, A. K. (editor), *1986 IEEE International Conference on Robotics and Automation*. IEEE, April 7-10, 1986.

[9] Leahy, M. B., Valavanis, K. P. and Saridis, G. N.
The Effects of Dynamics Models on Robot Control.
In *Proceedings of the 1986 IEEE Conference on Robotics and Automation.* IEEE, San Francisco, CA, April, 1986.

[10] Luh, J. Y. S., Walker, M. W. and Paul, R. P.
Resolved-Acceleration Control of Mechanical Manipulators.
IEEE Transactions on Automatic Control 25(3):468-474, June, 1980.

[11] Markiewicz, B. R.
Analysis of the Computed-Torque Drive Method and Comparision with the Conventional Position Servo for a Computer-Controlled Manipulator.
Technical Memorandum 33-601, Jet Propulsion Laboratory, Pasadena, CA, March, 1973.

[12] Paul, R. P.
Robot Manipulators : Mathematics, Programming and Control.
MIT Press, Cambridge, MA, 1981.

[13] Schmitz, D., Khosla, P. K. and Kanade, T.
Development of CMU Direct-Drive Arm II.
In Hasegawa, Yukio (editor), *Proceedings of the 15-th International Symposium on Industrial Robotics.* Tokyo, Japan, September, 11-13, 1985.